DOI: 10.65731/ama/2026-0014

THE INFLUENCE OF TITANIUM ADDITION ON THE HIGH-TEMPERATURE OXIDATION BEHAVIOUR OF THE $Al_{0.7}CoCrFeNi$ ALLOY

Marzena TOKAREWICZ*, Kamila ZUBA, Wojciech Jerzy NOWAK**, Malgorzata GRADZKA-DAHLKE***

*Faculty of Mechanical Engineering, Bialystok University of Technology, Wiejska 45 C, 15-351 Bialystok
**Faculty of Mechanical Engineering and Aeronautics, Rzeszow University of Technology, Powstancow Warszawy 12, 35-959 Rzeszow

marzena.tokarewicz@sd.pb.edu.pl, k.zuba@prz.edu.pl, w.nowak@prz.edu.pl, m.dahlke@pb.edu.pl

received 20 December 2025, revised 31 January 2026, accepted 15 February 2026

Abstract: In recent years, the development of advanced materials capable of withstanding extreme environments has become a key focus in materials science and engineering. High-entropy alloys (HEAs) are increasingly recognized as promising candidates for high-temperature applications due to their unique compositional flexibility and exceptional thermal stability. This study investigates the influence of titanium addition on the microstructure and oxidation resistance of the $Al_{0.7}CoCrFeNi$ alloy, as titanium is known to affect diffusion processes and oxide scale stability at high temperatures. Alloys with different titanium contents (x = 0.05, 0.2, 0.5) were synthesised using the arc melting method and tested for high-temperature oxidation at 1000 °C for up to 1000 hours. Microstructural analysis revealed that low titanium additions ($x \leq 0.2$) had minimal impact on the alloy's biphasic, lamellar-dendritic structure, while higher titanium content (x = 0.5) led to significant morphological changes and elemental segregation. Results of oxidation kinetics showed that alloys with low titanium content maintained excellent oxidation resistance due to the formation of a stable Al_2O_3 layer. In contrast, the alloy with x = 0.5 exhibited rapid weight gain and poor oxidation resistance, attributed to the formation of porous, multilayered oxide scales dominated by Ti and Cr oxides. These findings suggest that while minor titanium additions do not significantly compromise oxidation resistance, excessive Ti content disrupts the formation of protective oxide layers, potentially limiting the alloy's suitability for extreme temperature environments.

Key words: high-entropy alloys, $Al_{0.7}CoCrFeNi$, HEA, high-temperature oxidation, titanium

1. INTRODUCTION

The continuous advancement of technology generates a growing demand for novel materials with increasingly superior properties. One such area of interest involves materials designed to work under high-temperature conditions, particularly in industrial sectors such as aerospace, nuclear energy, and the oil and gas industry. In the case of components such as thermal and jet engines, efficiency increases with rising operating temperatures [1]. Therefore, it is crucial to search for materials that exhibit enhanced high-temperature performance compared to those commonly used today.

High-entropy alloys (HEAs) have emerged as a promising response to this demand, attracting significant scientific interest due to their vast potential in both functional and structural material applications. Existing studies indicate that many HEA compositions are characterized by high melting points, excellent phase stability, and outstanding mechanical properties at elevated temperatures [2–5]. These alloys are typically composed of a minimum of five principal elements in equal or near-equal atomic proportions. The incorporation of alloying additives is also feasible, enabling the development of a significantly broader range of compositions than is possible with conventional alloy design approaches [6, 7]. This, in turn, provides a wide scope for tailoring their properties to meet specific application requirements.

The AlCoCrFeNi alloy was one of the first HEAs to be thoroughly investigated, and its mechanical properties have proven to be promising [8–10]. Its ability to maintain good properties at elevated temperatures makes it a potential candidate to replace currently used nickel-based superalloys [11, 12], whose operating temperatures are limited to approximately 1300 °C [13]. Numerous studies in the literature have examined the properties of this alloy and the effects of varying its constituent elements [14–17]. Among these, aluminum has the most significant influence: increasing its content leads to a phase transformation from face-centered cubic (fcc) to a mixture of fcc and body-centered cubic (bcc), and then to a fully bcc structure. This transformation results in increased hardness but reduced ductility of the alloy [18, 19]. The aluminum content in the $Al_xCoCrFeNi$ alloy also affects its high-temperature oxidation resistance-higher concentrations promote the formation of a continuous Al_2O_3 layer, thereby improving oxidation resistance [20].

The $Al_{0.7}CoCrFeNi$ alloy represents a compromise between ductility and hardness; however, there is a limited number of studies dedicated to this specific composition [21–24]. Mohanty et al. [25] compared the high-temperature oxidation resistance and microhardness of $Al_{0.3}CoCrFeNi$ and $Al_{0.7}CoCrFeNi$ high-entropy alloys fabricated via laser cladding. The alloy with higher aluminum content exhibited a microhardness of approximately 380 HV, whereas the lower aluminum variant showed a hardness of around 170 HV. In the $Al_{0.3}CoCrFeNi$ alloy, oxidation led to the formation of a thick external Cr_2O_3 layer and a discontinuous Al_2O_3 subscale in the form of coarse precipitates. Increasing the aluminum contribution resulted in a thinner Cr_2O_3 scale and the development of a continuous Al_2O_3 layer, whose thickness increased with oxidation time, thereby enhancing the alloy's oxidation resistance. Some researchers highlight the potential to modify the functional properties of that HEAs by adding specific elements in appropriate amounts-for

example, molybdenum and vanadium to increase strength [26, 27], manganese to improve corrosion resistance [28], and silicon to enhance wear resistance [29].

It was decided to study the effect of titanium addition on this alloy, since according to the literature it can improve oxidation resistance at high temperatures. Liang et al. [30] studied the effect of titanium content on the oxidation behaviour of $AlCoCrNiTi_x$ high-entropy alloys at 900 °C. The results showed that an alloy containing $Ti_{0.1}$ exhibited optimal behaviour, reducing the oxidation rate by two orders of magnitude and promoting the formation of a protective α-Al_2O_3 layer, highlighting the crucial role of Ti in stabilizing the oxide scale and preventing its spallation. The sample without titanium exhibited irregular oxidation, resulting in an incomplete oxide layer with numerous pores. In contrast, the oxides formed on the $Ti_{0.1}$, $Ti_{0.4}$, $Ti_{0.7}$, and $Ti_{1.0}$ samples were well-developed and primarily composed of Al_2O_3, with an increasing contribution of Cr_2O_3. In the AlCrFeNiTi alloy, initial selective oxidation occurs between Ti atoms on the alloy surface and oxygen from the test atmosphere, leading to the formation of an outer TiO_2 layer that limits further oxygen diffusion into the alloy. Subsequently, the oxygen present within the alloy reacts selectively with Al atoms, resulting in the formation of an underlying α-Al_2O_3 sublayer [31]. The beneficial effect of titanium on high-temperature oxidation has also been confirmed for other high-entropy alloys [32, 33].

The results of this study make a valuable contribution to the broader understanding of the high-entropy $Al_{0.7}CoCrFeNi$ alloy, particularly regarding its oxidation resistance at elevated temperatures. By analyzing the alloy's response to oxidizing environments, this work provides insight into the complex interactions between its multi-element composition and the formation of protective oxide scales. According to the literature, the incorporation of titanium into the alloy matrix can influence the oxidation mechanism not only by altering the thermodynamic stability of the oxide phases but also by modifying the diffusion pathways of reactive elements as well as their activities. The present research significantly expands the current knowledge of titanium's effect on the high-temperature oxidation behaviour of the $Al_{0.7}CoCrFeNi$ alloy and lays the groundwork for future studies aimed at optimizing its performance in demanding thermal environments.

2. MATERIALS AND METHODS

The chemical composition of studied high entropy alloys (HEA) was selected based on thermodynamical calculations of phase stabilities performed using CALPHAD. Stability of phases was calculated using ThemoCalc software. Projected chemical composition of $Al_{0.7}CoCrFeNiTi_x$ (x=0.05, 0.2, 0.5) HEAs are given in Table 1. In the following, $Al_{0.7}CrFeCoNi$ will be identified as the reference alloy (Ref), and the others depending on the titanium content will be called Ref+0.05Ti, Ref+0.2Ti and Ref+0.5Ti, respectively.

Tab. 1. Projected chemical composition of studied HEAs

Alloys	Element [at. %]					
	Al	Co	Cr	Fe	Ni	Ti
Ref	14.89	21.28	21.28	21.28	21.28	-
Ref+0.05Ti	14.74	21.05	21.05	21.05	21.05	1.05
Ref+0.02Ti	14.28	20.41	20.41	20.41	20.41	4.08
Ref+0.5Ti	13.46	19.23	19.23	19.23	19.23	9.62

HEAs were produced by ARC-Melting method. At the first step high purity powders (purity over 99.99%) were weighted and mixed using ball mill for 2 hours to ensure a uniform powder distribution. Such prepared powders mixtures were pressed into pellets with diameters of 15 mm and height approximately 12 mm using Herzog hydraulic press made by Siemens. Such prepared pellets were melted in ARC-Melter furnace made by Edmund Buehler by following procedure. Prior melting reaction chamber was triple pumped down up to $2\cdot10^{-2}$ mbar pressure using oil pump and flushed by argon with 5N purity. After third flushing high vacuum at level of $5\cdot10^{-5}$ mbar is produced using diffusion pump. After reaching of pressure $5\cdot10^{-5}$ mbar reaction chamber is fulfilled with small amount Ar to ensure occurrence of plasma. After such preparation arc-melting process itself is done. The arc melting is processed till the pellets are completely melted through. After complete melting of pellets they were turned around by 180° and remelted again. Such procedure was repeated 4 times to ensure uniform distribution of chemical composition through the sample. After melting procedure samples were cooled down with the furnace in the Ar atmosphere. After this samples were removed from the furnace and further cooled down to room temperature. From such prepared alloys rectangular samples with dimensions of 10 x 10 x 5 mm were machined. All surface of cut specimens were ground up to 1200 grit sand paper. Ground specimens were cleaned using ethanol in ultrasonic cleaner prior exposure to high temperature. High temperature oxidation tests were performed in Nabertherm SN 313602 furnace at temperature 1000 °C up to 1000 hours of exposure in laboratory air. After oxidation for 24, 100 and 1000 hours mass change of each sample was measured using microbalance KERN ABT 120-4M made of KERN & SOHN GmbH with accuracy of 10^{-4} g to elucidate the oxidation kinetics. To ensure the oxidation results repeatability two samples per each alloy type were exposed. The oxidation tests were performed under isothermal conditions without thermal cycling. After reaching the required oxidation time, selected samples were removed and cooled to room temperature in ambient air prior to mass measurements. No oxide scale spallation during cooling was observed. Minor cracking and local spallation visible in some samples are most likely related to sample handling between analytical procedures. Only minor discrepancies were observed, thus no error bars were introduced to the mass change plot. After oxidation sample surfaces were observed by SEM in terms of formed oxide scales morphology. Selected samples were subjected to chemical composition measurement using glow discharge optical emission spectrometer (GD-OES). The intensity of light emission as function of sputtering time was obtained. The results were recalculated to show concentration expressed in at. % as function of sputtering time using so-called relative sensitivity factors (RSF). Quantification procedure was described elsewhere [34–36]. After GD-OES measurement samples surfaces were sputtered by gold and electroplated with Ni coating to protect oxide scale from damage during cross-sections preparation and to ensure good contrast between oxide scale and the resin. Cross-sections for SEM observation were prepared using standard metallographic procedure with the last step of polishing using 0.05µm grain dimensions. Cross-sections were analyzed using Phenom XL scanning electron microscope equipped with EDS detector to investigate the chemical composition of formed oxide scales and HEA microstructures as well as for elemental mappings showing elements distribution over the investigated surfaces shown in BSE images.

DOI: 10.65731/ama/2026-0014

3. RESULTS AND DISCUSSION

3.1. Microstructure of the studied alloys

Measured chemical composition of obtained $Al_{0.7}CoCrFeNiTi_x$ (x=0, 0.05, 0.2, 0.5) HEAs is given in Table 2. A comparison between the chemical compositions of the obtained alloys (Table 2) and the designed compositions (Table 1) reveals a close agreement. The most significant differences are observed in the aluminum content, which is likely due to the evaporation of this element during the melting process, as aluminum has the lowest melting point among the alloying elements [37].

Tab. 2. Measured chemical composition of studied HEAs

Alloys	Element [at. %]					
	Al	Co	Cr	Fe	Ni	Ti
Ref	13.5	21.1	22.1	21.9	21.4	-
Ref+0.05Ti	13.2	19.9	22.5	21.9	21.3	1.3
Ref+0.02Ti	12.9	18.9	22.1	21.5	20.5	4.2
Ref+0.5Ti	11.8	21.5	19.1	19.0	18.6	10.0

Figure 1 shows representative SEM images of the microstructures of the investigated materials at 5000x magnification. This magnification was chosen due to the extremely fine dispersion of microstructural features, which are smaller than one micrometer. The microstructure of the Ref alloy without titanium (Fig. 1a) is typical for this class of high-entropy alloys with a molar aluminum content below 1. In the case of the reference alloy, the microstructure was previously described in detail by Nowak [38] as lamellar-dendritic. Two highly refined phases can be distinguished, corresponding to A2 and B2 crystal structures, which differ in the concentration of the main alloying elements [39]. The addition of titanium in the amount of 0.05 had virtually no effect on the alloy's microstructure, except for a further refinement of the individual phases (Fig. 1b). At a titanium content increased to 0.2, the dendritic morphology is replaced by grains containing a plate-like mixture of phases (Fig. 1c). In contrast, the microstructure of the Ref+0.5Ti sample differs significantly. A mosaic-like structure is observed, characterized by pronounced elemental segregation within phase precipitates located in the intergranular regions. Similar microstructures were reported for the AlCrFeNiTi alloy without cobalt in the study by Zhi [40].

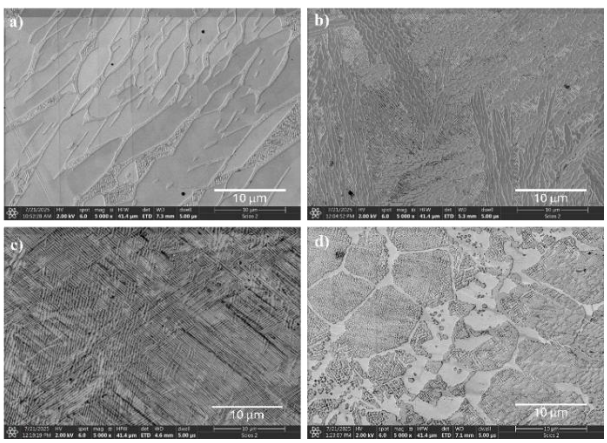

Fig. 1. SEM micrographs of tested alloys: a) Ref, b) Ref+0.05Ti, c) Ref+0.2Ti, d) Ref+0.5Ti

3.2. Oxidation kinetics

Figure 2 presents curves illustrating the relative mass changes of the investigated materials during air exposure at 1000 °C up to 1000 h. For the Ref alloy, the mass change remains minimal even after 1000 hours of exposure in air, indicating excellent resistance to high-temperature oxidation. Its weight gain after 1000 h of exposure reach about 0.2 $mg \cdot cm^{-2}$. The addition of titanium in the amounts of 0.05 and 0.2 results in only a slight increase in weight gain, with the curves following a similar trend to that of the base alloy. Similar correlations for the AlCoCrFeNi alloy were reported by Butler [20]; however, in that case, the relative mass change after 100 hours of high-temperature oxidation at 1050 °C was approximately ten times greater, which may have been due to differences in sample surface preparation. The samples were ground to a 1200 grit SiC surface finish, cleaned with acetone/isopropanol, and placed in annealed alumina boats prior to oxidation testing. In contrast, Li et al. [12] observed even greater relative mass changes when investigating the effect of copper addition on the high-temperature oxidation behaviour of a similar alloy.

Surprisingly, the Ref+0.5Ti alloy exhibited significantly higher mass change after air exposure at 1000 °C up to 1000 h. Within the first 24 hours, the weight gain of the samples was more than ten times higher than that of the titanium-free alloy and those with lower titanium content. Although the oxidation rate decreased in the subsequent hours of the test, the weight gain remained substantially higher compared to the other investigated materials. This result indicates that the oxidation products in this case do not provide effective protection. A similar negative effect of increased titanium content on the oxidation kinetics of AlCoCrNi alloys (without Fe) was reported by Liang [30]. In contrast, Zhang et al. [33] observed the opposite trend for $CoCrMoNbTi_x$ alloys (without aluminum) used as laser-cladded coatings, where increasing titanium content led to a reduction in weight gain. These differences are attributed to the composition and quality of the oxide layers formed on the sample surfaces.

In this context, a detailed analysis of the oxide phases formed during high-temperature exposure appears to be particularly important.

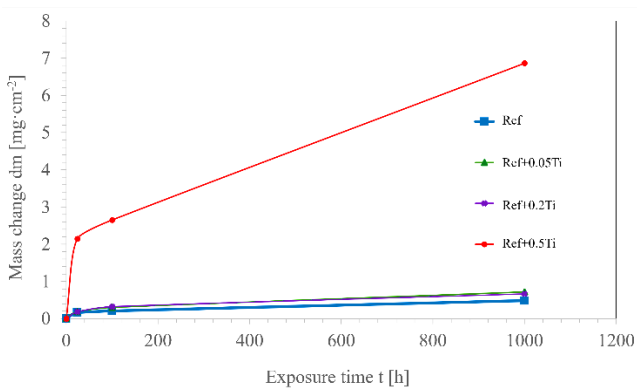

Fig. 2. Oxidation kinetics curves of the tested alloys

3.3. GD-OES analysis

The obtained results of glow discharge optical emission spectrometry analysis of the investigated materials revealed significant

differences in the chemical composition of the surface layers after high-temperature oxidation, resulting from the modification of the alloy composition through titanium addition. A graphical representation is provided in Figure 3.

After 1000 hours of high-temperature oxidation of the Ref alloy (Fig. 3a), aluminum diffusion to the sample surface is clearly observed. The aluminum concentration changes with the oxygen content, indicating the formation of an aluminum oxide layer on the surface. Only at the depth of the layer corresponding to approximately 500-800 seconds of sputtering time is a slight depletion of aluminum compared to the bulk material, due to the diffusion of Al atoms to the surface. In contrast, the concentrations of the other alloying elements in the surface layer are significantly lower, what indicates formation of relatively pure Al_2O_3 oxide scale.

The GD-OES profile of the Ref+0.05Ti alloy (Fig. 3b) indicates more intense elemental diffusion compared to the base alloy. The oxide layer is thicker, as evidenced by the deeper oxygen penetration. The surface is composed almost exclusively of aluminum oxide, while the concentrations of other metallic elements in the surface layer are significantly below 1 at.%.

In the case of the Ref+0.2Ti alloy (Fig. 3c), the GD-OES profile shows a similar trend. However, a slightly higher presence of alloying elements is observed in the surface layer-approximately 1 at. % for chromium and iron, and around 0.2 at. % for nickel and cobalt. Titanium diffusion to the surface is also clearly visible.

In contrast, increasing the titanium content to 0.5 mol leads to a distinct change in the oxide layer composition after just 100 hours of oxidation (Fig. 3d). The surface is dominated by titanium and chromium oxides, while aluminum oxide is located beneath the outermost layer.

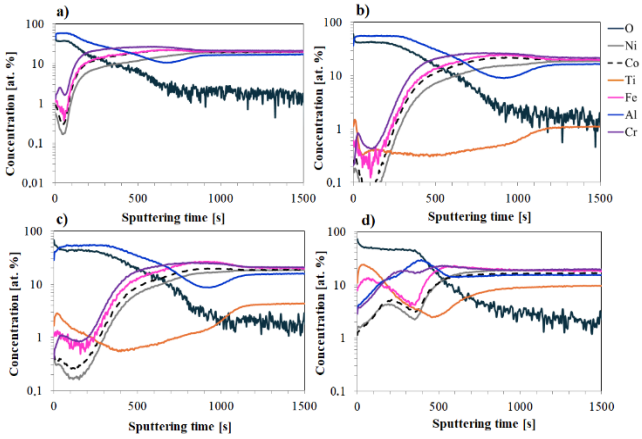

Fig. 3. GD-OES profiles of tested alloys after air oxidation: a) Ref for 1000 h, b) Ref+0.05Ti for 1000 h, c) Ref+0.2Ti for 1000 h, d) Ref+0.5Ti for 100 h

The evolution of GD-OES profiles during the oxidation process of individual materials provides further insight into the surface oxide layer transformations. Figures 4–6 illustrate the evolution of surface composition in the Ref alloy and in the Ref+0.2Ti and Ref+0.5Ti alloys after 24, 100, and 1000 h of oxidation.

For the Ref alloy (Fig. 4), the profiles differ only in the thickness of the oxide layer, which increases with oxidation time. The surface is dominated by aluminum and oxygen, with their concentrations decreasing with sputtering time. Beneath the aluminum oxide layer, a noticeable depletion of aluminum is observed compared to the bulk material, indicating the diffusion of atoms of this element to the surface. The concentrations of the other alloying elements increase toward the core of the sample.

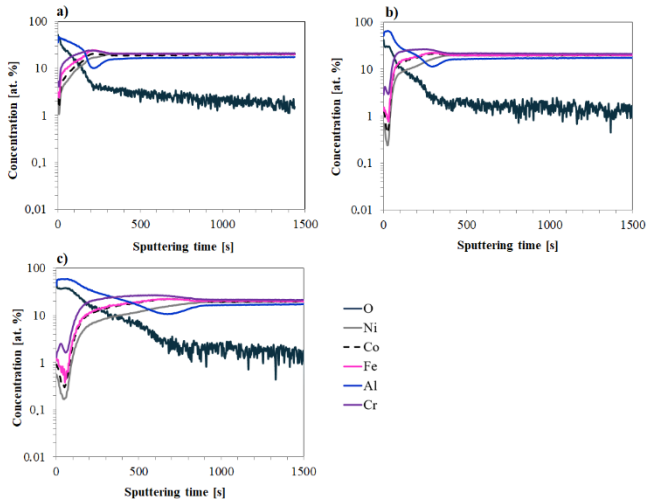

Fig. 4. GD-OES profiles of the Ref alloy after air oxidation for: a) 24 h, b) 100 h, c) 1000 h

In contrast, the titanium profile exhibits distinct behaviour. In the oxide layer, titanium content is significantly lower than in the bulk, but a pronounced increase is observed at the surface, suggesting titanium diffusion through the aluminum oxide layer to the surface (Fig. 5).

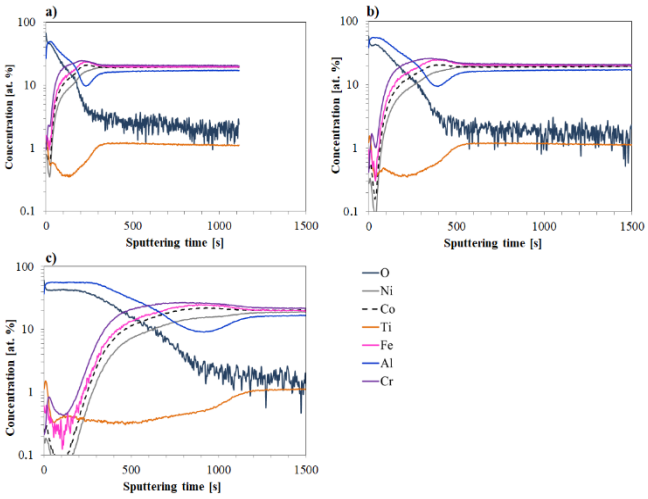

Fig. 5. GD-OES profiles of the Ref+0.2Ti alloy after air oxidation for: a) 24 h, b) 100 h, c) 1000 h

Figure 6 shows GD-OES profiles for the Ref+0.5Ti alloy after 24 and 100 hours of oxidation (Fig. 6a and 6b, respectively). After 24 hours at 1000°C (Fig. 6a), the surface contains complex oxides of the alloying elements, with iron and titanium being predominant. These oxides are gradually replaced by chromium oxides at greater depths. Aluminum content increases only near the interface with the bulk material. After 100 hours of oxidation (Fig. 6b), the surface oxide layer becomes thinner, likely due to spallation, and is composed mainly of titanium and iron oxides. Toward the core, the concentrations of these elements decrease, while cobalt and nickel contents slightly increase. Al-enrichment is found at the oxide scale-base alloy interface (in the region where oxygen profile drops down - Fig. 6b), which can suggest formation of internal zone rich

DOI: 10.65731/ama/2026-0014

in Al-oxides or Al-rich oxide subscale.

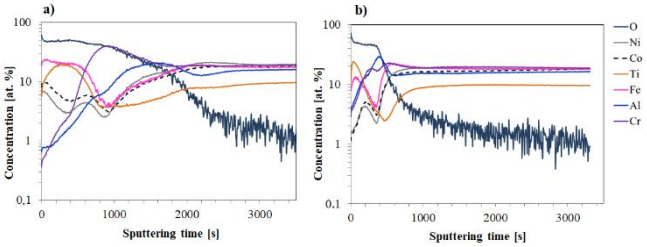

Fig. 6. GD-OES profiles of the Ref+0.5Ti alloy after air oxidation for: a) 24 h, b) 100 h

3.4. Surface morphology of the oxide layer

Figures 7-10 present microscopic images of the surfaces of the investigated materials after 1000 hours of high-temperature oxidation at 1000 °C. For direct comparison, Figure 11 presents the oxidation surface morphologies of all investigated alloys at the same magnification (x1000). On the surface of the Ref sample, an almost uniform aluminum oxide layer is observed, which is locally delaminated and cracked. Only in a few areas can bright spots be seen, corresponding to complex oxides of nickel, cobalt, and iron (Fig. 7e, g, h).

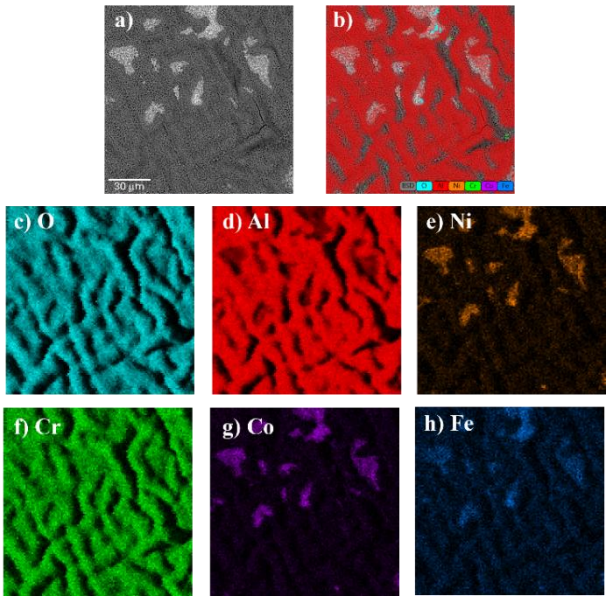

Fig. 7. Morphology of an oxide scale of the Ref sample after air oxidation for 1000 h: a) SEM image, b) combined map EDS, c-h) mapping of elements

The surface of the Ref+0.05Ti alloy also exhibits a dominant Al_2O_3 layer. Locally, small precipitates of oxides rich in Ni and Co are visible, along with numerous titanium oxides (Fig. 8).

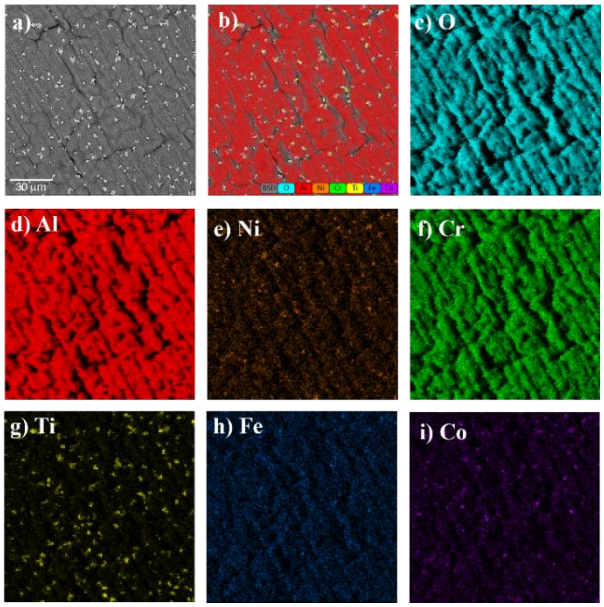

Fig. 8. Morphology of an oxide scale of the Ref+0.05Ti sample after air oxidation for 1000 h: a) SEM image, b) combined map EDS, c-i) mapping of elements

A similar surface morphology is observed for the Ref+0.2Ti alloy after high-temperature oxidation (Fig. 9). The sample surface reveals a continuous Al_2O_3 layer with numerous titanium oxide precipitates, as well as less frequent oxides of Co, Ni, and Fe.

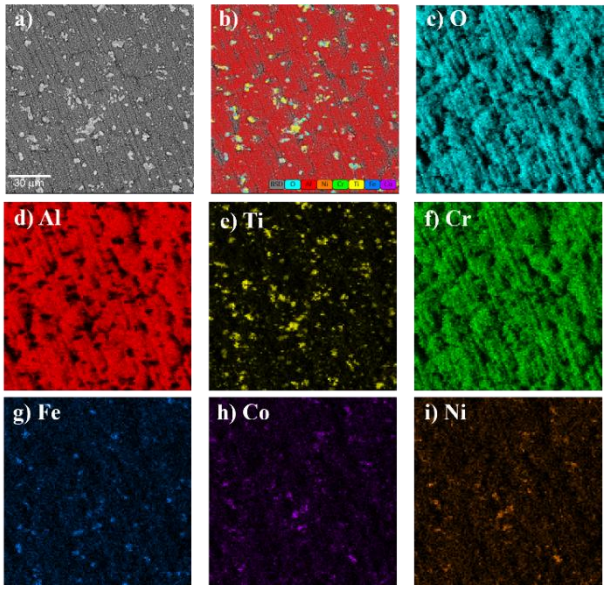

Fig. 9. Morphology of an oxide scale of the Ref+0.2Ti sample after air oxidation for 1000 h: a) SEM image, b) combined map EDS, c-i) mapping of elements

In contrast, the surface morphology of the Ref+0.5Ti sample appears entirely different. There is practically no aluminium in the outer oxide layer (Fig. 10b). The surface is dominated by complex oxides of Ni, Co, and Cr, along with large clusters of titanium-rich oxides (Fig. 10d).

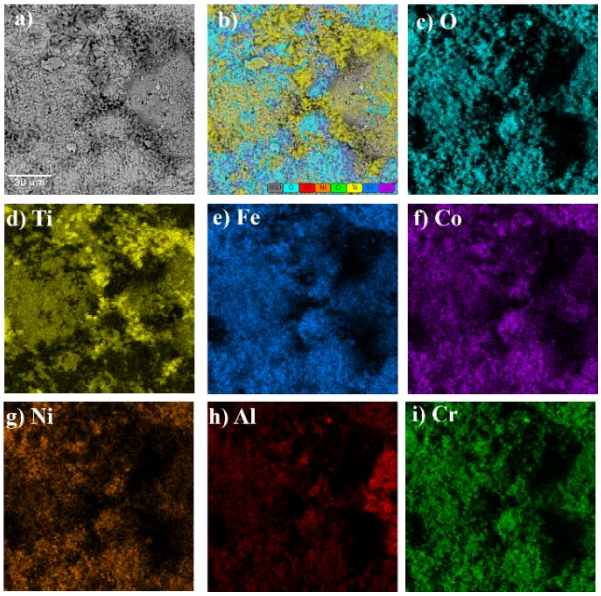

Fig. 10. Morphology of an oxide scale of the Ref+0.5Ti sample after air oxidation for 1000 h: a) SEM image, b) combined map EDS, c-i) mapping of elements

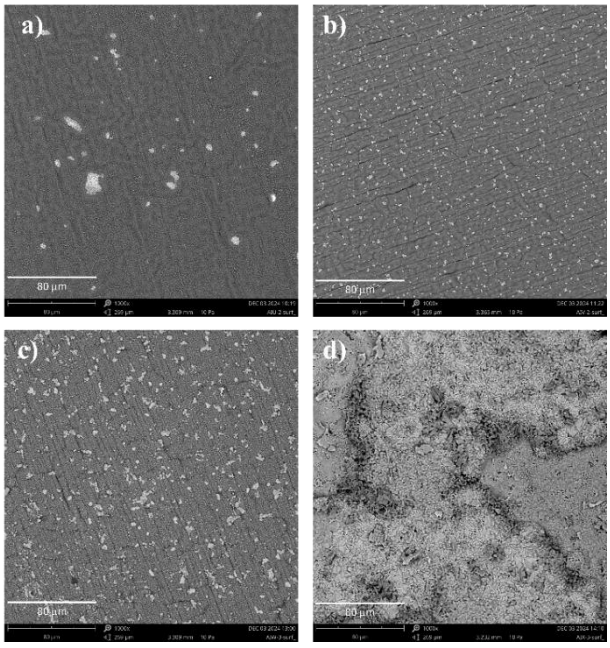

Fig. 11. SEM surface morphologies of oxidized alloys after 1000 h: a) Ref, b) Ref+0.05Ti, c) Ref+0.2Ti, d) Ref+0.5Ti, magnification: x1000

3.5. Cross-section of the oxide layer

The cross-sectional analysis of the samples after oxidation confirms the surface morphology observations. On the surface of the Ref alloy without titanium, exposure to high-temperature oxidation resulted in the formation of a thin, compact Al_2O_3 layer, which protects the metallic substrate from further oxidation (Fig. 12). Beneath the alumina layer, a single-phase region depleted in aluminum is observed. As the Al_2O_3 scale forms, the interdendritic phase rich in aluminum disappears from the subsurface structure. With prolonged high-temperature exposure, the thickness of both layers increases slightly. Microstructural coarsening is also evident (Fig. 12a-c). These findings are supported by EDS elemental mapping of the alloy's constituent elements (Fig. 13).

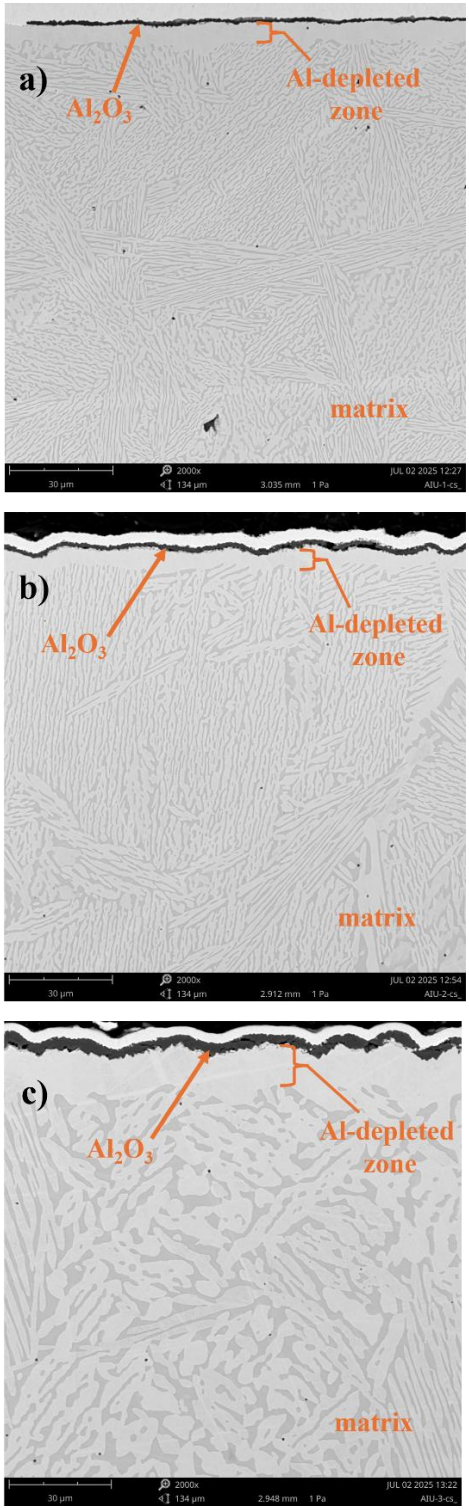

Fig. 12. Microstructure of the cross-section of the Ref sample after air oxidation for a) 24h, b) 100h, c) 1000h

A similar situation is observed in the cross-sectional images of the Ref+0.05Ti alloy samples (Fig. 14). On the surface of the materials exposed to high-temperature oxidation, only thin, compact Al_2O_3 layers are visible, adjacent to a metallic sublayer depleted in aluminum. With increasing exposure time, the thickness of both layers slightly increases, and microstructural coarsening becomes

DOI: 10.65731/ama/2026-0014

noticeable (Fig. 14 a-c). The chemical composition of all phases is illustrated in Figure 15.

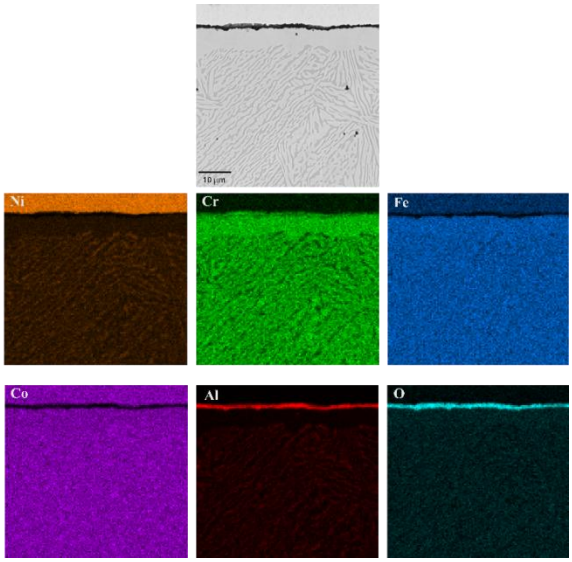

Fig. 13. EDS elemental maps of the cross-section of the Ref sample after air oxidation for 24 h

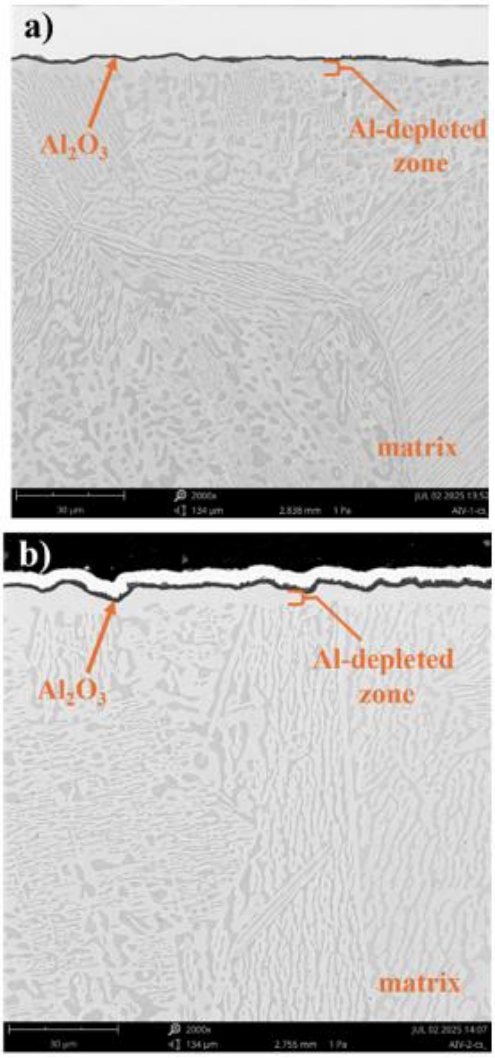

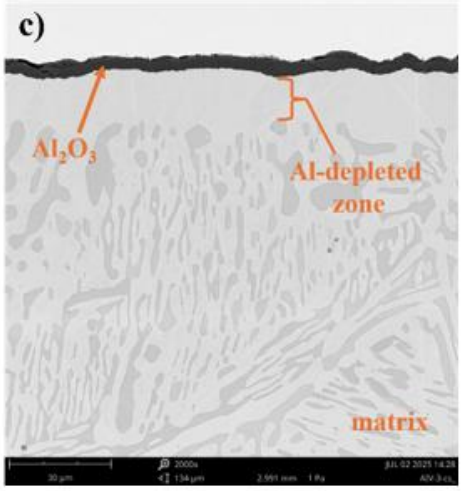

Fig. 14. Microstructure of the cross-section of the Ref+0.05Ti sample after air oxidation for a) 24h, b) 100h, c) 1000h

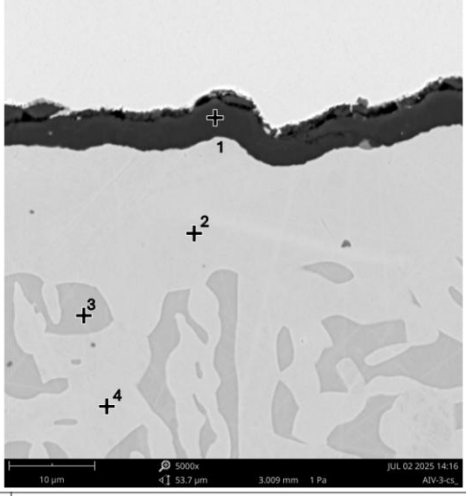

No	Element [at.%]						
	Oxygen	Aluminium	Cobalt	Chromium	Iron	Nickel	Titanium
1	65.75	34.25	-	-	-	-	-
2	-	7.09	22.30	28.51	25.90	16.20	-
3	-	34.52	16.42	7.31	10.02	29.06	2.67
4	-	7.09	22.47	28.22	25.99	16.23	-

Fig. 15. EDS point analysis of the cross-section of the Ref+0.05Ti sample after air oxidation for 1000 h

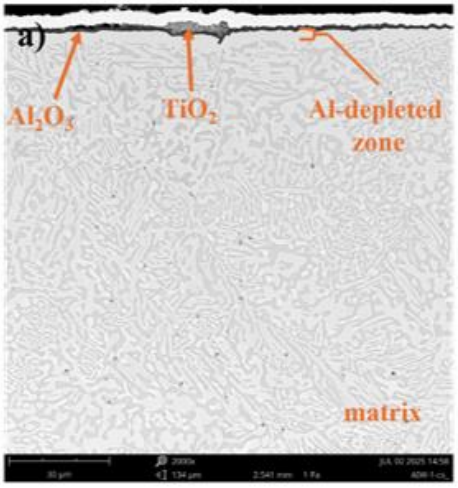

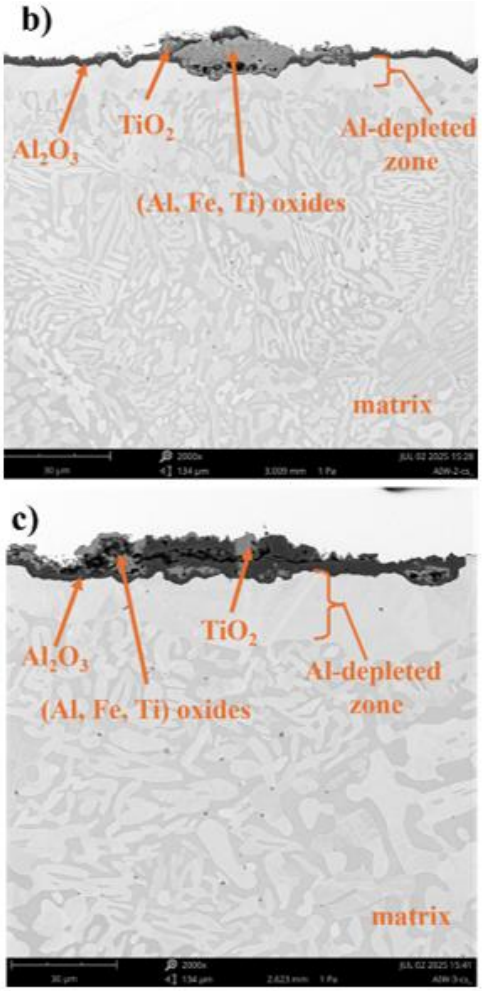

Fig. 16. Microstructure of the cross-section of the Ref+0.2Ti sample after air oxidation for a) 24 h, b) 100 h, c) 1000 h

A continuous Al_2O_3 layer also formed on the surface of the Ref+0.2Ti alloy. Beneath it, an aluminum-depleted layer is present (Fig. 16a–c). Locally, clusters of oxides with a porous structure and diverse chemical composition appear on the surface (Fig. 17a, b).

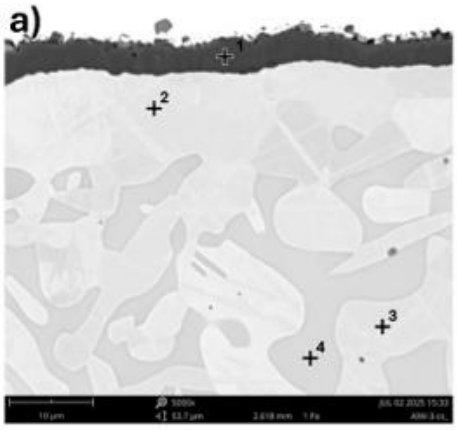

No	Element [at.%]						
	Oxygen	Aluminium	Cobalt	Chromium	Iron	Nickel	Titanium
1	65.39	34.61	-	-	-	-	-
2	-	6.20	21.44	28.29	27.33	16.74	-
3	-	6.16	21.18	28.00	27.13	16.05	1.49
4	-	29.67	19.05	5.64	8.29	26.93	10.42

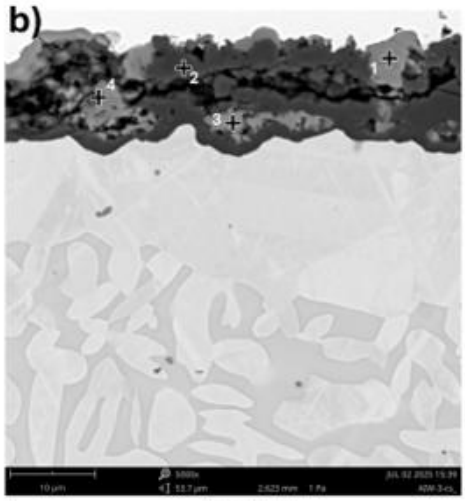

No	Element [at.%]						
	Oxygen	Aluminium	Cobalt	Chromium	Iron	Nickel	Titanium
1	71.05	34.61	1.58	0.70	8.39	-	12.00
2	66.45	33.55	-	-	-	-	-
3	68.94	17.82	5.15	2.24	2.35	3.20	-
4	78.72	9.80	1.64	-	3.91	1.17	4.75

Fig. 17. EDS point analysis of the cross-section of the Ref+0.2Ti sample after air oxidation for 1000 h a) continuous Al_2O_3 layer, b) cross-section of complex oxide precipitates

The cross-section images of the Ref+0.5Ti alloy samples differs significantly and confirms the surface morphology analysis of this material (Fig. 18a–c). After 24 hours of high-temperature exposure, a thick oxide layer (~10 µm) forms on the sample surface, clearly divided into three regions with distinct chemical compositions. An outer spinel layer can be distinguished, followed by a layer of Cr and Al oxides containing Ti. At the interface with the metallic matrix, a thin Al_2O_3 layer is visible, indicating internal oxidation of aluminum. This interface is irregular and undulated, which may promote oxide delamination (Fig. 18a). In Figure 18b, showing the cross-section after 100 hours of oxidation, the oxide layer is significantly thinner, suggesting delamination of porous oxides. Locally, complex multilayered oxide structures with high porosity can be observed. After 1000 hours of high-temperature exposure, the oxide layer becomes thick (~30 µm) and porous (Fig. 18c).

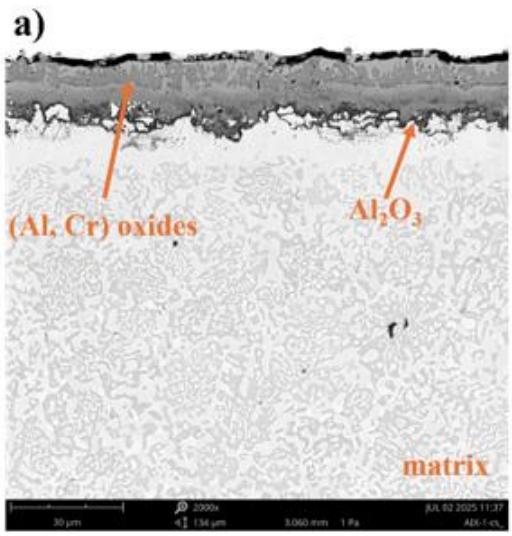

DOI: 10.65731/ama/2026-0014

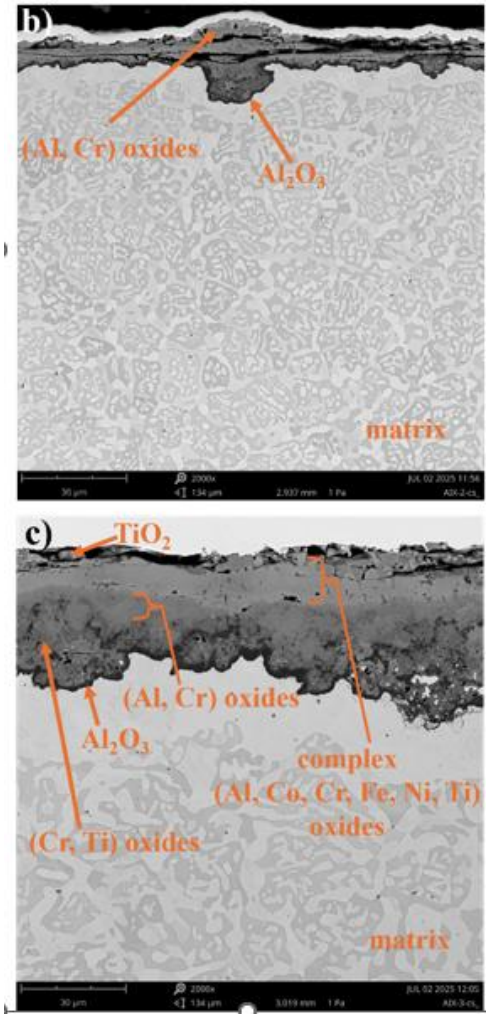

Fig. 18. EDS point analysis of the cross-section of the Ref+0.5Ti sample after air oxidation for 1000 h a) continuous Al_2O_3 layer, b) cross-section of complex oxide precipitates

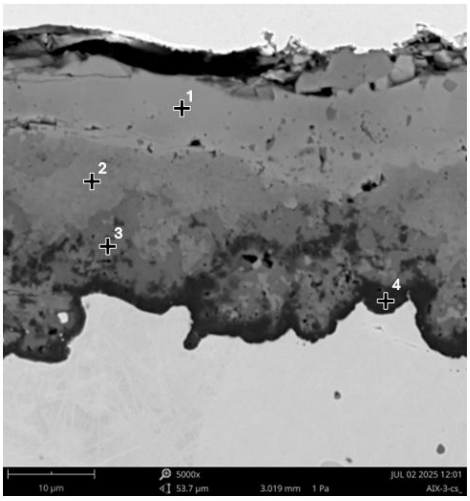

No	Element [at.%]						
	Oxygen	Aluminium	Cobalt	Chromium	Iron	Nickel	Titanium
1	68.29	5.58	6.04	6.22	7.82	4.99	1.05
2	75.58	7.74	-	16.11	-	-	0.58
3	71.60	11.70	-	7.83	-	-	8.87
4	65.46	34.54	-	-	-	-	-

Fig. 19. EDS point analysis of the cross-section of the Ref+0.5Ti sample after air oxidation for 1000 h

In the oxide layer formed after 1000 hours of high-temperature exposure, four sublayers with distinct chemical compositions can be identified (Fig. 19). The outermost layer is structurally homogeneous and contains all alloying elements in approximately equal proportions (Fig. 19, point 1). Beneath it lies a thin layer of Cr oxides with some Al content (point 2). Below this is a porous spinel layer with a high Ti content (point 3). The innermost oxide layer is composed of Al_2O_3 (point 4). Similar layered oxide structures were observed by Jalowicka and Nowak [41] after oxidation of a titanium-containing nickel-base superalloy for 20 hours in synthetic air at 1050 °C.

The phenomenon of internal oxidation of aluminum in AlCoCrFeNi alloys without titanium has also been described by Butler [20, 42]. In turn, Zhi-Sheng Nong [40] investigated high-temperature oxidation of a similar AlCrFeNiTi alloy (without Co, but with Ti) at 900 °C. The oxidation process was characterized as consisting of two mechanisms: oxygen diffusion into the oxide layer and outward diffusion of alloying elements to the surface. In this case as well, the presence of titanium did not improve high-temperature oxidation resistance; sample mass increased steadily with exposure time up to 100 hours. As a result, a Ti-rich oxide layer formed on the surface, while the Al_2O_3 layer was located beneath it. Similar findings regarding the influence of titanium on the oxidation behaviour of the AlCrMoNbTi alloy were reported by Zhang [32, 33].

4. CONCLUSION

The obtained results clearly indicate that a small addition of titanium (up to x = 0.2) in the Ref alloy has only a minor effect on its microstructure and high-temperature oxidation behaviour.

The microstructures of the Ref, Ref+0.05Ti, and Ref+0.2Ti alloys do not differ qualitatively. In all cases, the structure can be described as biphasic, lamellar-dendritic. Only a refinement of the individual phase constituents is observed with increasing titanium content. Similarly, in high-temperature oxidation tests, the influence of titanium addition up to x = 0.2 can be considered as causing only a slight deterioration in oxidation resistance. The relative weight gains follow a trend similar to that of the unmodified alloy over 1000 hours of testing, which is associated with the formation of a protective, stable, and compact Al_2O_3 layer on the surface. The formation of this layer is accompanied by the development of a subsurface aluminum-depleted zone. For all the discussed alloys, the thickness of both layers increases slightly with prolonged high-temperature exposure. Microstructural coarsening is also observed. In the case of alloys with titanium additions up to 0.2, isolated precipitates of oxides of other alloying elements appear on the surface, which tend to delaminate, potentially contributing to a slight reduction in oxidation resistance.

In contrast, the changes occurring in the Ref+0.5Ti alloy are qualitatively significant. The microstructure transforms into a mosaic-like structure with numerous intermetallic phase precipitates located in the intergranular regions. The oxidation behaviour is also markedly different. Even during the first 24 hours of exposure at 1000 °C, no protective Al_2O_3 layer is observed. Instead, a layer of oxides of the alloying elements forms on the surface, which readily delaminates. Aluminum tends to oxidize internally. As a result, oxide weight gain occurs rapidly. Prolonged high-temperature exposure leads to significant thickening of the oxide layer, further chemical segregation within the oxide sublayers, and continued rapid mass increase of the sample.

In summary, if specific functional property requirements (e.g., wear resistance) for the Ref alloy suggest the addition of titanium, it is recommended-based on high-temperature oxidation behaviour-to limit its content to a maximum of 0.2.

REFERENCES

1. Dewangan SK, Mangish A, Kumar S, Sharma A, Ahn B, Kumar V. A review on High-Temperature Applicability: A milestone for high entropy alloys. Eng Sci Technol Int J. 2022;35:101211.
2. Dixit S, Rodriguez S, Jones MR, Buzby P, Dixit R, Argibay N, et al. Refractory High-Entropy Alloy Coatings for High-Temperature Aerospace and Energy Applications. J Therm Spray Technol. 2022;31(4):1021–31.
3. Praveen S, Kim HS. High-Entropy Alloys: Potential Candidates for High-Temperature Applications – An Overview. Adv Eng Mater. 2018;20(1):1700645.
4. Lim KR, Lee KS, Lee JS, Kim JY, Chang HJ, Na YS. Dual-phase high-entropy alloys for high-temperature structural applications. J Alloys Compd. 2017;728:1235–8.
5. Miracle D, Miller J, Senkov O, Woodward C, Uchic M, Tiley J. Exploration and Development of High Entropy Alloys for Structural Applications. Entropy. 2014;16(1):494–525.
6. George EP, Raabe D, Ritchie RO. High-entropy alloys. Nat Rev Mater. 2019;4(8):515–34.
7. Gao MC, Yeh JW, Liaw PK, Zhang Y. High-Entropy Alloys: Fundamentals and Applications. Springer International Publishing; 2016.
8. Yeh JW, Chen SK, Lin SJ, Gan JY, Chin TS, Shun TT, et al. Nanostructured High-Entropy Alloys with Multiple Principal Elements: Novel Alloy Design Concepts and Outcomes. Adv Eng Mater. 2004;6(5):299–303.
9. Wang FJ, Zhang Y, Chen GL, Davies HA. Cooling rate and size effect on the microstructure and mechanical properties of AlCoCrFeNi high entropy alloy. J Eng Mater Technol. 2009;131(3):034501.
10. Chou HP, Chang YS, Chen SK, Yeh JW. Microstructure, thermophysical and electrical properties in AlxCoCrFeNi (0≤x≤2) high-entropy alloys. Mater Sci Eng B. 2009;163(3):184–9.
11. Chen J, Zhou X, Wang W, Liu B, Lv Y, Yang W, et al. A review on fundamental of high entropy alloys with promising high–temperature properties. J Alloys Compd. 2018;760:15–30.
12. Li M, Zhang H, Zeng Y, Liu J. A perspective on investigating transition metal high-entropy alloys for high-temperature applications. Acta Mater. 2022;240:118313.
13. Pollock TM, Tin S. Nickel-Based Superalloys for Advanced Turbine Engines: Chemistry, Microstructure and Properties. J Propuls Power. 2006;22(2):361–74.
14. Bhattacharya R, Annasamy M, Cizek P, Kamaraj M, Muralikrishna GM, Hodgson P, et al. Evolution of phase constitution with mechanical alloying and spark plasma sintering of nanocrystalline AlxCoCrFeNi (x = 0, 0.3, 0.6, 1 mol) high-entropy alloys. J Mater Res. 2022;37(4):959–75.
15. Feng XB, Fu W, Zhang JY, Zhao JT, Li J, Wu K, et al. Effects of nanotwins on the mechanical properties of AlxCoCrFeNi high entropy alloy thin films. Scr Mater. 2017;139:71–6.
16. Guo L, Xiao D, Wu W, Ni S, Song M. Effect of Fe on microstructure, phase evolution and mechanical properties of (AlCoCrFeNi)100-xFex high entropy alloys processed by spark plasma sintering. Intermetallics. 2018;103:1–11.
17. López Ríos M, Socorro Perdomo PP, Voiculescu I, Geanta V, Crăciun V, Boerasu I, et al. Effects of nickel content on the microstructure, microhardness and corrosion behavior of high-entropy AlCoCrFeNix alloys. Sci Rep. 2020;10(1):21119.
18. Cao T, Shang J, Zhao J, Cheng C, Wang R, Wang H. The influence of Al elements on the structure and the creep behavior of AlxCoCrFeNi high entropy alloys. Mater Lett. 2016;164:344–7.
19. Joseph J, Jarvis T, Wu X, Stanford N, Hodgson P, Fabijanic DM. Comparative study of the microstructures and mechanical properties of direct laser fabricated and arc-melted AlxCoCrFeNi high entropy alloys. Mater Sci Eng A. 2015;633:184–93.
20. Butler TM, Weaver ML. Oxidation behavior of arc melted AlCoCrFeNi multi-component high-entropy alloys. J Alloys Compd. 2016;674:229–44.
21. Liu G, Liu L, Liu X, Wang Z, Han Z, Zhang G, et al. Microstructure and mechanical properties of Al0.7CoCrFeNi high-entropy-alloy prepared by directional solidification. Intermetallics. 2018;93:93–100.
22. Lu J, Chen Y, Zhang H, He L, Mu R, Shen Z, et al. Y/Hf-doped Al0.7CoCrFeNi high-entropy alloy with ultra oxidation and spallation resistance at 1200 °C. Corros Sci. 2020;174:108803.
23. Gwalani B, Wang T, Jagetia A, Gangireddy S, Muskeri S, Mukherjee S, et al. Dynamic Shear Deformation of a Precipitation Hardened Al0.7CoCrFeNi Eutectic High-Entropy Alloy Using Hat-Shaped Specimen Geometry. Entropy. 2020;22(4):431.
24. Tokarewicz M, Gradzka-Dahlke M, Nowak WJ, Gradzik A, Szala M, Walczak M. Effect of Vanadium Addition on the Wear Resistance of Al0.7CoCrFeNi High-Entropy Alloy. Materials. 2024;17(23):6021.
25. Mohanty A, Sampreeth JK, Bembalge O, Hascoet JY, Marya S, Immanuel RJ, et al. High temperature oxidation study of direct laser deposited AlXCoCrFeNi (X=0.3,0.7) high entropy alloys. Surf Coat Technol. 2019;380:125028.
26. Zhu JM, Fu HM, Zhang HF, Wang AM, Li H, Hu ZQ. Microstructures and compressive properties of multicomponent AlCoCrFeNiMox alloys. Mater Sci Eng A. 2010;527(26):6975–9.
27. Dong Y, Zhou K, Lu Y, Gao X, Wang T, Li T. Effect of vanadium addition on the microstructure and properties of AlCoCrFeNi high entropy alloy. Mater Des. 2014;57:67–72.
28. Abdi F, Aghajani H, Asl SK. Evaluation of the corrosion resistance of AlCoCrFeMnNi high entropy alloy hard coating applied by electro spark deposition. Surf Coat Technol. 2023;454:129156.
29. Liu H, Sun S, Zhang T, Zhang G, Yang H, Hao J. Effect of Si addition on microstructure and wear behavior of AlCoCrFeNi high-entropy alloy coatings prepared by laser cladding. Surf Coat Technol. 2021;405:126522.
30. Liang M, Zhang J, Gao J, Yi H, Yin B, Yang Z, et al. Enhancing the oxidation resistance of AlCoCrNi high-entropy alloy via Ti-induced microstructural modifications. Corros Sci. 2025;246:112746.
31. Nong ZS, Lei YN, Zhu JC. Wear and oxidation resistances of AlCrFeNiTi-based high entropy alloys. Intermetallics. 2018;101:144–51.
32. Zhang J, Wu Q, Yang C, Yang Z, Yin B, Yang Y. Initial oxidation behavior of AlCrMoNbTi high-entropy alloys studied by DFT calculations and experiments. Intermetallics. 2025;176:108549.
33. Zhang S, Qi W, Zhang R. Effect of Ti content on wear and high-temperature oxidation resistances of laser-clad CoCrMoNbTix high-entropy alloy coatings. Mater Lett. 2023;345:134490.
34. Pfeifer JP, Holzbrecher H, Quadakkers WJ, Breuer U, Speier W. Quantitative analysis of oxide films on ODS-alloys using MCs+-SIMS and e-beam SNMS. Fresenius J Anal Chem. 1993;346(1):186–91.
35. Quadakkers WJ, Elschner A, Speier W, Nickel H. Composition and growth mechanisms of alumina scales on FeCrAl-based alloys determined by SNMS. Appl Surf Sci. 1991;52(4):271–87.
36. Nowak WJ. Characterization of oxidized Ni-based superalloys by GD-OES. J Anal At Spectrom. 2017;32(9):1730–8.
37. Wang D, Liu Z, Liu W. Experimental measurement of vacuum evaporation of aluminum in Ti–Al, V–Al, and Ti6Al4V alloys by electron beam. Metals. 2021;11(11):1688.
38. Nowak WJ, Kubaszek T, Gradzik A, Grądzka-Dahlke M, Perkowski D, Tokarewicz M, et al. Effect of Ti Doping of Al0.7CoCrFeNi-Based High Entropy Alloys on Their Erosion Resistance by Solid Particles. Materials. 2025;18(14):3328.
39. Jalowicka A, Nowak W, Naumenko D, Singheiser L, Quadakkers W j. Effect of nickel base superalloy composition on oxidation resistance in SO2 containing, high pO2 environments. Mater Corros. 2014;65(2):178–87.
40. Butler TM, Pavel MJ, Weaver ML. The effect of annealing on the microstructures and oxidation behaviors of AlCoCrFeNi complex concentrated alloys. J Alloys Compd. 2023;956:170391.

DOI: 10.65731/ama/2026-0014

The research leading to these results has received funding from the commissioned task entitled "VIA CARPATIA Universities of Technology Network named after the President of the Republic of Poland Lech Kaczynski" contract no. MEiN/2022/DPI/2578 action entitled "ISKRA – building inter-university research teams".

Marzena Tokarewicz: https://orcid.org/0000-0002-6620-5282

Kamila Zuba: https://orcid.org/0009-0005-5328-1314

Wojciech J. Nowak: https://orcid.org/0000-0002-5285-4900

Malgorzata Gradzka-Dahlke: https://orcid.org/0000-0001-5566-3002

This work is licensed under the Creative Commons BY-NC-ND 4.0 license.